

A NEW DETERMINATION OF THE PROTON MAGNETIC MOMENT IN TERMS OF THE  
 NUCLEAR MAGNETON TO WITHIN  $4.3 \times 10^{-5}\%$

B. A. MAMYRIN, N. N. ARUEV and S. A. ALEKSEENKO

A. F. Ioffe Physico-technical Institute, USSR Academy of Sciences

Submitted February 3, 1972

Zh. Eksp. Teor. Fiz. 63, 3-20 (July, 1972)

A new method is reported for the determination of the proton magnetic moment in terms of the nuclear magneton ( $\mu_p/\mu_n$ ) to within  $4.3 \times 10^{-5}\%$  using a resonance magnetic mass spectrometer with a special two-section ion source. The method eliminates almost completely the effect of stray electric fields on the measured proton cyclotron frequency, which has not been achieved by other methods. The proton spin precession frequency, necessary for the determination of  $\mu_p/\mu_n$ , is measured with an NMR probe placed in the same magnetic field in which the proton cyclotron frequency is determined. A description is given of the apparatus and experimental procedure. All sources of random and systematic errors are discussed and evaluated. An account is given of control experiments which have confirmed the estimated errors. The result of 11 series of measurements is (without correction for the diamagnetic shielding of protons in water):  $\mu_p/\mu_n = 2.7927744 \pm 0.0000012$  ( $4.3 \times 10^{-5}\%$ ).

## I. INTRODUCTION

ACCURATE values of the fundamental constants (electron mass and charge, proton mass and charge, the Faraday, Avogadro, Planck, and Boltzmann constants, and so on) can be obtained from a relatively small number of quantities which can be measured directly with high precision. The proton magnetic moment expressed in nuclear magnetons ( $\mu_p/\mu_n$ ) occupies an important place among them.<sup>[1,2]</sup> The precision with which this quantity has been measured has been steadily increasing in recent years, and since its determination reduces to the measurement of the ratio of two frequencies (the NMR frequency  $\omega_n$  and the cyclotron frequency  $\omega_c$  of protons) in the same magnetic field, it may be expected that  $\mu_p/\mu_n$  will become one of the most accurately measured quantities in physics.

The last evaluation of all experimental data on fundamental constants was reported by Taylor, Parker and Langenberg in 1969,<sup>[1]</sup> who showed that the main contradiction lay in the fact that the most precise measured value of  $\mu_p/\mu_n$  available at the time<sup>[3]</sup> was not in agreement with the Faraday constant  $F$  obtained by Craig et al.<sup>[4]</sup> Despite the fact that this measurement of  $F$  raised certain doubts as to the electrochemical method employed, and even though this was a single de-

termination, Taylor et al accepted it as satisfactory and rejected the  $\mu_p/\mu_n$  data although the result reported in<sup>[3]</sup> was well confirmed by the very serious work reported in<sup>[5]</sup>.

Subsequent events showed the decision of Taylor et al was clearly incorrect, since the values of  $\mu_p/\mu_n$  obtained in different countries<sup>[6-8]</sup> turned out to be in full agreement with<sup>[3]</sup>. The International Commission on Fundamental Constants, chaired by E. R. Cohen, is currently engaged upon the gathering of data for a new determination of the most probable values of the fundamental constants, which it proposes to establish in the course of 1972.

In view of the existing situation there is clearly a need for a new high-precision determination of  $\mu_p/\mu_n$ .

The ratio of the proton magnetic moment  $\mu_p$  =  $\omega_{\text{NMR}} \hbar / 4\pi H$  to the nuclear magneton  $\mu_n = e\hbar / 4\pi M_p c$  is

$$\mu_p / \mu_n = \omega_{\text{NMR}} / \omega_c,$$

where  $\omega_{\text{NMR}}$  is the NMR frequency of the proton in a uniform field  $H$ , and  $\omega_c = eH / M_p c$  is the proton cyclotron frequency in the same field  $H$ .

There are three existing methods for  $\mu_p/\mu_n$ . They differ only by the method used to determine  $\omega_c$ . The NMR frequency is measured in all these methods with

very high precision, using proton probes (water, oil) placed in the same magnetic field in which  $\omega_c$  is determined.<sup>[9]</sup>

In the first method for  $\mu_p/\mu_n$  the frequency  $\omega_c$  is measured with the aid of the omegatron.<sup>[5,6,8]</sup> In the second method,  $\omega_c$  is measured by means of the time-of-flight analyzer and a static sector mass spectrometer which is traversed successively by the same ions.<sup>[7]</sup> In the third method the ratio  $\mu_p/\mu_n$  is measured with the resonance magnetic mass spectrometer (RMMS).<sup>[3,10,11]</sup>

The essential difficulty in increasing the precision of  $\omega_c$  (and hence of  $\mu_p/\mu_n$ ) is the disturbing effect of stray electric fields in the ion drift space on the motion of the ions. These fields are largely due to contact phenomena, space charges, and the polarization of metal walls intercepting ions and electrons. They cannot be completely eliminated and therefore all three methods make use of the so-called extrapolation technique whereby measurement of  $\omega_c$  for ions of different mass are used to calculate a precise value of  $\omega_c$  for protons. Theoretical analysis of this problem<sup>[3,12]</sup> shows that the extrapolation technique yields an accurate result only when the stray electric-field distribution in the ion drift space remains the same for ions with different  $M/q$ . Unfortunately, this condition was not satisfied in any of the above three methods for  $\omega_c$ .

Measurement of  $\omega_c$  with the aid of the RMMS has two main advantages over the other two methods. Firstly, since  $\omega_c$  is measured during a single revolution on an orbit of large radius, the magnetic field can be determined accurately at all points on the orbit, and the correction for a possible field inhomogeneity can be found. Secondly, the use of an electron multiplier, and the comparatively low ion-current losses during ion transit through the instrument, enable low ion currents to be used, and this substantially reduces the uncertainty associated with any violation of the above condition for the applicability of the extrapolation technique. However, it has been found that changes in stray electric fields may affect the final value of  $\mu_p/\mu_n$  obtained in this way. This was seen in the increased spread of the extrapolated values of  $\mu_p/\mu_n$  which was the main source of uncertainty in<sup>[3,11]</sup>.

The main reason for the change in the stray fields within the RMMS is the change in the current distribution in the ion beams and the change in the position of these beams when  $\omega_c$  for ions with different  $M/q$  is determined.

The conclusion therefore is that if the extrapolation technique is to be valid (and the condition for this is that electric fields due to space charges and polarization potentials must remain unaltered), all the potentials in the source must remain constant. This cannot be achieved with an instrument using a conventional ion source when it is adjusted for ions with different  $M/q$ .

## II. RMMS WITH A TWO-SECTION ION SOURCE

The change in the stray fields mentioned above can be avoided if the ions are generated in the RMMS by a source consisting of two, three, or more sections, with ionizing and accelerating gaps in each section, in which ions with two or more values of  $M_n/q_n$  are produced in

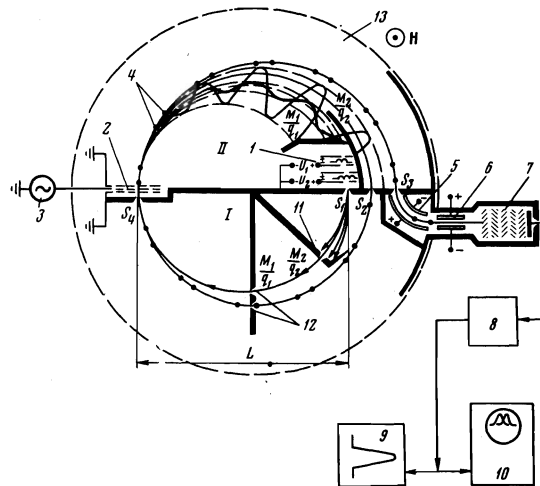


FIG. 1. Schematic illustration of the analyzer of the resonance magnetic mass spectrometer with two-section ion source. 1—Ion source, 2—modulator, 3—high-frequency oscillator, 4—ion packets, 5—cylindrical capacitor, 6—plane capacitor, 7—multiplier, 8—electrometer, 9—pen recorder, 10—oscillograph, 11—screen mounted at an angular distance of  $45^\circ$  from the source, 12—screen with aperture slits, 13—magnet pole piece. Slit sizes:  $S_1 = 0.4 \times 8.0$  mm,  $S_2 = 0.4 \times 6.0$  mm,  $S_3 = 6.0$  mm,  $S_4 = 1.0 \times 1.0$  mm.

different sections. Ions then leave the source with different energies corresponding to the accelerating potentials in the different sections, and can reach the modulator slit simultaneously at constant source-electrode potentials. Since measurements on two types of ion (two values of  $M/q$ ) are sufficient to enable us to obtain the extrapolation line, we have adopted the simplest solution, i.e., the two-section ion source.

The operation of the RMMS using a single-section ion source, and of the installation for the determination of  $\mu_p/\mu_n$  as a whole, was described in detail elsewhere<sup>[3,10]</sup> and will not be considered here. The RMMS with the two-section ion source is shown schematically in Fig. 1 and differs from the earlier system<sup>[3,10]</sup> only by the presence of the second source section. The source is shown in greater detail in Fig. 2.

It consists of two sources, placed end to end, in which ionization is produced by electron impact. The electrons are emitted by tungsten coils 1 and 6 (Fig. 2) each of which consists of 11 turns of  $75 \mu$  diameter wire. The inside diameter of the coil is 0.3 mm. The electrons are accelerated through 150–200 V and ionize He, Ne, and Ar gas molecules. The electron beams travel parallel to the magnetic lines of force, which focus them, and are eventually collected by electron collectors. Ions produced in each ionizing gap (2, 7) are ejected by the positive reflector plates 3 and 8 and are accelerated in the gaps 4 and 9. Since the ion-orbit radius at exit from the source should be half the distance between the exit source slit and the modulator slit  $L$  (Fig. 1), i.e.,

$$r = 144 H^{-1} \sqrt{U_n M_n / q_n} = 0.5 L$$

and the magnetic is assumed constant ( $H \approx 1200$  Oe), the accelerating voltages within the gaps must satisfy the condition

$$U_1 M_1 / q_1 = U_2 M_2 / q_2.$$

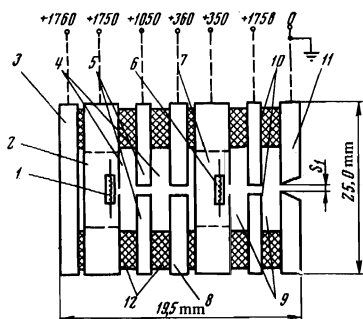


FIG. 2. Schematic illustration of the two-section ion source (viewed from above): 1—hot filament for section I, 2—ionizing gap of section I, 3—reflecting electrode of section I, 4—first accelerating gap, 5—first horizontally deflecting electrodes, 6—hot filament for section II, 7—ionizing gap of section II, 8—reflecting electrode of section II, 9—second accelerating gap, 10—second horizontally deflecting electrodes, 11—grounded electrode with source exit slit  $S_1$ , 12—porcelain insulators. The potentials indicated at the top of the figure correspond to the situation where section I produces  $\text{He}_4^+$  ions and section II produces  $\text{Ne}_{20}^+$  ions.

Horizontally deflecting plates 5 and 10 are used to correct the ion beam trajectories at the source exit. They are maintained at potentials of roughly half the accelerating potential per gap, and can be controlled independently.

The exit slits of the ionizing gaps, the exit slit  $S_1$ , and the slit in the second reflector are covered by fine copper grids which reduce the electric field distortion within the accelerating gaps. The first section (the most distant from the grounded plate carrying slit  $S_1$ ) operates at a high constant accelerating voltage  $U_1 \approx 1750$  V and produces an  $\text{He}^+$  beam. The second section operates at lower potentials and produces beams of  $\text{Ne}_{20}^+$ ,  $\text{Ne}_{20}^+$ , and  $\text{Ar}_{40}^+$  ions ( $U_2 = 700, 350,$  and  $175$  V respectively). The latter section can be used as a single-section source producing beams with different  $M/q$ .

The source control panel is provided with a facility for discrete switching of voltages corresponding to different values of  $M/q$  and final fine adjustment of these voltages.

Tests have shown that the two sections produce comparable ion-beam currents (a few units of  $10^{-9}$  A). The helical cathodes require heating currents of 1–1.05 A, and the electron currents from these cathodes are kept at 3 mA.

The two-section source thus produces simultaneously one of the following three pairs of ion beams:  $\text{He}_4^+ - \text{Ne}_{20}^+$ ,  $\text{He}_4^+ - \text{Ne}_{20}^+$ , or  $\text{He}_4^+ - \text{Ar}_{40}^+$ . In each case the radii of the ion orbits at the modulator slit are equal.

In contrast to our previous method,<sup>[3]</sup> transition from  $M/q = 4$  to  $M/q = 10$  (or 20 and 40) requires only a change in the modulator frequency and amplitude which, however, does not affect any of the source potentials, so that all the stray electric fields in the drift space (region I in Fig. 1), produced by space charges and polarization potentials due to ions leaving the source, remain unaltered. In principle, the stray fields between the modulator and drift slit (region II) may be altered when the instrument is adjusted for different  $M/q$ . There are, however, a number of factors which ensure that this effect is practically unnoticeable.

Firstly, there is a considerable difference between

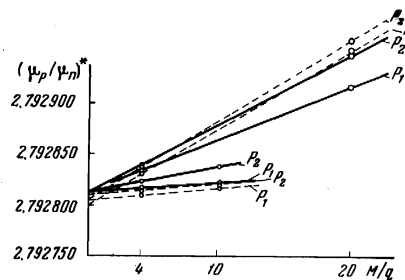


FIG. 3. The ratio  $(\mu_p/\mu_n)^*$  as a function of the pressure of the analyzed gases (He and Ne) when the RMMS incorporates the two-section source (solid line) and when it operates with a one-section source (broken lines).  $P_1 = 5 \times 10^{-6}$  Torr,  $P_2 = 8 \times 10^{-6}$  Torr.

the radial modulation depths of the resonant and non-resonant ion orbits, so that screens can be used to eliminate virtually completely the effect that the space charge due to the nonresonant ions exerts on resonant ions executing orbits that pass through the drift slit  $S_2$ .

Secondly, the highest polarization potentials are produced at those points which intercept well-focused ion beams with considerable ion currents. In the space behind the modulator the ions are energy (radius) modulated and this is equivalent to geometric defocusing, with the attendant sharp reduction in the ion currents at the shields and in the drift space (compared with the current density at exit from the source). Stray electric fields in region II (behind the modulator, Fig. 1) are therefore very low as compared with region I (between the source and the modulator).

To verify that the stray fields in the RMMS chamber remained constant when the two-section source was employed, we performed a series of control experiments designed to establish the effect of the different factors on the ratio  $\mu_p/\mu_n$ . We measured  $(\mu_p/\mu_n)_i^*$  for ions with different mass-to-charge ratio and then used the extrapolation technique to find  $(\mu_p/\mu_n)^*$  at zero mass.<sup>[12]</sup> The final result for the extrapolated  $(\mu_p/\mu_n)^*$  was accurate to within  $\pm 2 \times 10^{-5}\%$ .

1. The first control experiment involved changing the pressure in the chamber after the two points corresponding to  $(\mu_p/\mu_n)_i^*_{\text{He}_4^+}$  and  $(\mu_p/\mu_n)_i^*_{\text{Ne}_{20}^+}$  were recorded. In the case of the single ion source this pressure change leads to a large spread in the extrapolated  $(\mu_p/\mu_n)^*$  (Fig. 3). However, for the two-section source there is a change in the slope of the extrapolation lines but not in the extrapolated values of  $(\mu_p/\mu_n)^*$ , at least to within experimental error (Fig. 3).

2. The next control experiment showed that, to within experimental error, the extrapolated  $(\mu_p/\mu_n)^*$  was independent of the ratio of currents leaving the first and second sections, although here again there was a change in the slope of the extrapolation lines.

3. The effect of stray fields on the slope of the extrapolation lines is shown by the interesting experiment with the screen 11 (Fig. 1) which was placed at an angular distance of  $45^\circ$  to the source. The extrapolation lines for  $\text{He}_4^+ - \text{Ne}_{20}^+$  and  $\text{He}_4^+ - \text{Ne}_{20}^+$  had slopes of a different sign before and after the introduction of the screen, respectively (Fig. 4). The negative slope of the  $\text{He}_4^+ - \text{Ne}_{20}^+$  line shows that the introduction of the second

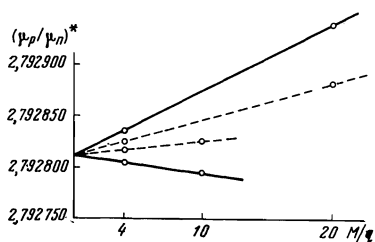


FIG. 4. Effect of the screen on the slope of the extrapolation lines when the RMMS operates with the two-section source. Solid line—prior to insertion of screen, broken line—after insertion of screen.

section of the source, with an accelerating potential corresponding to  $\text{Ne}_{20}^{+}$  ions, ensures that ions with high  $M/q$  (for example,  $\text{H}_2\text{O}^+$ ,  $\text{O}^+$ , and  $\text{N}^+$ ) produce strong electric fields in the region of the slit 12 which lies at an angular distance of  $90^\circ$  from the source (this slit restricts the angular width of the working ion beam).

When the screen 11 was introduced to shield the working ion beam from the effect of stray fields due to residual-gas ions, the slope of the  $\text{He}_4^+ - \text{Ne}_{20}^{+}$  line was reduced while that of the  $\text{He}_4^+ - \text{Ne}_{20}^{+}$  line became positive (Fig. 4), but the extrapolated  $(\mu_p/\mu_n)^*$  remained unaltered.

4. Control experiments were also performed to establish the effect of stray fields in the ion drift space (between modulator 2 and drift slit  $S_2$ ; Fig. 1, region II). It was found that this effect was negligible in comparison with the corresponding effect in region I. The actual procedure was to determine  $(\mu_p/\mu_n)^*$  for each of the three ion pairs as a function of the modulating voltage. A change in the modulation conditions leads to a change in the stray fields in region II, since there is an attendant change in the energy spread of ions passing through the modulator. The effect of the change in the stray fields in region II was not, however, noticeable within our precision.

Analysis of the operation of the mass spectrometer with the two-section source has thus shown that the basic condition for the validity of the extrapolation method, i.e., constant stray-field distribution in the RMMS chamber during measurement of the cyclotron frequency of two types of ion, was satisfied with a high degree of accuracy.

### III. APPARATUS

There was a sharp reduction in the spread of extrapolated  $\mu_p/\mu_n$  values when the new source was introduced, and it became desirable to reduce other sources of error too. This involved a modification of all the systems within the measuring installation described previously.<sup>[3,10]</sup> The new arrangement is illustrated in Fig. 5. The central part of the installation is the RMMS whose principle of operation is described in detail elsewhere.<sup>[3]</sup> Here we shall confine our attention to the new features which have resulted in a substantial increase in measurement accuracy.

1. The stability of the magnetic field in time was sharply improved by introducing superstabilization of the magnetic flux in the magnet gap. This system consists of the end coils, the photocompensated amplifier F-116, the d.c. amplifier, and the correction coils

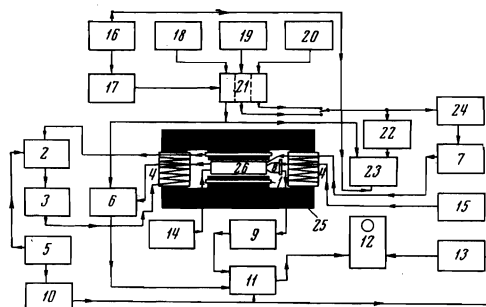


FIG. 5. Block diagram of the measuring system. Sweep and magnetic field superstabilization systems: 1—end coils, 2—photocompensated amplifier F-116, 3—d.c. amplifier, 4—actuating coils, 5—3 Hz sweep oscillator. Cyclotron resonance and NMR signal detection system: 6—NMR detector, 9—electrometric amplifier, 10—phase shifter, 11—switching unit, 12—oscilloscope, 13—sweep amplifier. Supply system for the RMMS analyzer: 14—power supply for the ion source, 15—power supply for the electron multiplier 8; 24, 7—frequency multiplier and power amplifier for the high-frequency oscillator. System for varying the frequency ratio: 16—quartz oscillator operating at 1 MHz, 17—frequency multiplier ( $\times 5$ ), 18—NMR signal generator ( $\approx 120$  kHz), 19—cyclotron resonance signal generator ( $\approx 650$  kHz), 20—cyclotron resonance signal generator ( $\approx 470$  kHz), 21—three-channel frequency mixer ( $\approx 5.12$ ,  $\approx 5.65$ ,  $\approx 4.53$  MHz), 22—frequency divider (1:1000), 23—frequency ratio measurement (ChZ-24), 25—permanent magnet, 26—chamber of the RMMS analyzer.

(Fig. 5). The change in  $\omega_n/\omega_c$ , i.e. the relative change in the field, was less than  $0.2 \times 10^{-4}\%$ . At the same time, provision was made for slight modulation of the field at 3 Hz in order to generate the cyclotron resonance and nuclear magnetic resonance signals.

2. Shimming and magnetic paints were used to increase sharply the spatial homogeneity of the magnetic field. The field on the circular ion-drift orbit (224 mm in diameter) does not deviate from the field at the center of the chamber, where the NMR detector is located, by more than  $\pm 7 \times 10^{-4}\%$ . This has enabled us to increase sharply the accuracy of the correction for the spatial inhomogeneity of the magnetic field.

3. We have developed a new system for the precise measurement magnetic-field inhomogeneities. This involves measurements of all three field components,<sup>[11]</sup>  $\Delta H_z$ ,  $\Delta H_\phi$ ,  $\Delta H_\rho$ , at 24 points on the orbit. The time necessary for determining the field chart has been sharply reduced, and this has enabled us to determine the field before and after each run.

4. The cross section of the ion beam was reduced from 4 to  $1.5 \text{ mm}^2$  in order to reduce the uncertainty in the measured effective magnetic field. The volume of the ampoule in the NMR detector used to measure the field on the ion drift orbit was also reduced for the same reason from 500 to  $60 \text{ mm}^3$  (the internal diameter of the water-filled spherical ampoule was 4.8 mm).

Measurement of the magnetic field gradients show that the magnetic field is uniform within the ion beam cross section to within better than  $10^{-5}\%$ .

5. The uncertainty in the correction for the change in the magnetic field produced when the chamber is introduced into the magnet gap was reduced to  $0.18 \times 10^{-4}\%$ .

The above improvements (items 1–5) have enabled us to calculate the correction for the deviation of the effec-

tive magnetic field on the ion drift orbit from the field at the point at which the NMR detector is located to an accuracy better than  $0.20 \times 10^{-4}\%$ .

6. A system has been developed for the direct determination in digital form of the ratio of the NMR and cyclotron resonance frequencies. The principle of this system is illustrated in Fig. 5. It incorporates quartz stabilization of the oscillators and has enabled us to reduce the uncertainty in the frequency ratio to  $10^{-5}\%$ .

7. To improve the filter properties of the power amplifier unit we have completely eliminated the effect of the modulating-voltage harmonics on the final result of the measurements.

8. A system has been developed for the automatic stabilization of the modulating-voltage amplitude, which has increased the stability of the cyclotron-resonance signal and has facilitated the superposition of the NMR and cyclotron resonance signals on the oscillograph screen.

9. The effect of the magnetic field due to the cathode current has also been completely eliminated by connecting the cathodes of the two-section ion source in opposition, and by introducing compensating conductors. The correction for the cathode current became less than  $10^{-5}\%$ .

The above measures have resulted in an improvement in the overall stability and accuracy of the measurements. The resolution of the instrument was thereby increased to 50 000 at half height, and the asymmetry of the cyclotron-resonance peak became less than  $1\%$ .

Figure 6 gives one of the oscillograms showing the superposition of the NMR and cyclotron-resonance peaks used in the measurements.

The results of measurements and the method used to obtain the final value of  $\mu_p/\mu_n$  are described below.

#### IV. EXPERIMENTAL DATA

A typical run consisted of measuring the NMR and cyclotron-resonance frequency ratio for the three ion pairs,  $\text{He}_4^+ - \text{Ne}_{20}^+$ ,  $\text{He}_4^+ - \text{Ne}_{20}^{2+}$ , and  $\text{He}_4^+ - \text{Ar}_{40}^+$ , followed by repeated measurement on  $\text{He}_4^+ - \text{Ne}_{20}^+$ . Three measurements were performed on each pair, for example,  $\text{He}_4^+ - \text{Ne}_{20}^+$ ,  $\text{He}_4^+ - \text{Ne}_{20}^{2+}$ , or  $\text{Ne}_{20}^+ - \text{He}_4^+ - \text{Ne}_{20}^{2+}$ .

The main measurement involved the determination of the frequency ratio for two channels of the mixer for which the NMR and cyclotron-resonance signals were superimposed at the center of the oscilloscope screen. About 6–8 frequency-ratio readings were usually taken for each point.

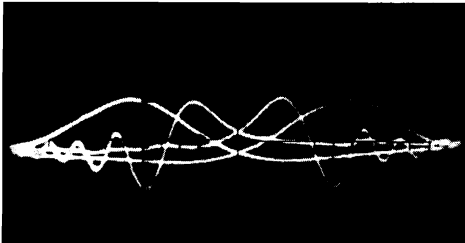


FIG. 6. Oscillogram showing the superposition of cyclotron resonance and NMR peaks. A change in the frequency of one of the signal generators (NMR or cyclotron resonance) by 1 Hz ( $\Delta f/f \approx 2 \times 10^{-7}$ ) distorts the symmetry of the central rhombus to a degree noticeable to the operator.

Since the magnetic field at the center of the mass-spectrometer chamber at which the NMR detector was located is different from the field on the working ion orbit, the magnetic-field distribution over the orbit is always determined before and after a working run.

For an ion with a given mass-to-charge ratio  $M_1/q_1$  the proton magnetic moment in nuclear magnetons was determined from the obtained frequency ratios of two mixer channels, with allowance for the fact that the measurements were made on the 196-th cyclotron-resonance harmonic, using the formula

$$(\mu_p/\mu_n)_i^* = \frac{\omega_n}{(\omega_{ci}/196)(M_1/M_p)(e/q_1)} = \frac{\omega_n}{\omega_{ci}} \frac{196M_p q_1}{M_1 e}, \quad (1)$$

where  $\omega_n/\omega_{ci}$  is the measured frequency ratio,  $M_p$  is the proton mass in atomic mass units,  $M_1$  is the ion mass in atomic mass units,  $e$  is the elementary charge, and  $q$  is the ion charge.

The atomic masses were taken from existing tabulations.<sup>[14]</sup> To determine the cyclotron-frequency shift due to stray electric fields, we used linear extrapolation to zero mass, employing the two values of  $(\mu_p/\mu_n)_i^*$  obtained for ions with different mass-to-charge ratio, beams of which were emitted simultaneously by the two-section source. In view of the low accuracy of the graphical extrapolation, the extrapolated value of  $(\mu_p/\mu_n)^*$  was obtained analytically for each ion pair. For example, for  $\text{He}_4^+ - \text{Ne}_{20}^{2+}$

$$(\mu_p/\mu_n)^* = (\mu_p/\mu_n)_{\text{He}_4^+}^* - \left( \frac{M_{\text{He}_4^+}}{M_{\text{Ne}_{20}^{2+}} - M_{\text{He}_4^+}} \right) [(\mu_p/\mu_n)_{\text{Ne}_{20}^{2+}}^* - (\mu_p/\mu_n)_{\text{He}_4^+}^*]. \quad (2)$$

A number of corrections have to be introduced before the true value of  $\mu_p/\mu_n$  can be deduced from  $(\mu_p/\mu_n)^*$ . These corrections are as follows.

#### 1. Correction for the Inhomogeneity of the Magnetic Field

Because of the inhomogeneity of the magnetic field the cyclotron period  $T_c$ , and hence the final value of  $\mu_p/\mu_n$  too, are different from those corresponding to the magnetic field  $H_0$  at the center of the chamber. The corresponding relative change in  $\mu_p/\mu_n$  is given by:<sup>[15]</sup>

$$\frac{\Delta(\mu_p/\mu_n)}{\mu_p/\mu_n} = \frac{\Delta T_c}{T_c} = \frac{1}{2\pi H_0} \left\{ \int_0^{2\pi} \left[ \frac{v_z(\varphi)}{v_\varphi} \Delta H_\varphi(\varphi) - \Delta H_z(\varphi) \right] (1 - \cos \varphi) d\varphi - \int_0^{2\pi} \frac{v_z(\varphi)}{v_\varphi} \sin \varphi \Delta H_\varphi(\varphi) d\varphi \right\}. \quad (3)$$

In this expression  $\Delta H_\varphi(\varphi)$ ,  $\Delta H_\rho(\varphi)$ , and  $\Delta H_z(\varphi)$  are the components of the magnetic-field vector at a point on the orbit, which is at an angular distance  $\varphi$  from the modulator,  $v_z(\varphi)$  is the vertical component of the ion-velocity vector, and  $v_\varphi$  is the main velocity of the ion corresponding to its motion along the working orbit. The velocity ratio  $v_z(\varphi)/v_\varphi$  under our conditions can be written in the form<sup>[13]</sup>

$$v_z(\varphi)/v_\varphi \approx \frac{1}{H_0} \int_0^\varphi \Delta H_\rho(\varphi) d\varphi. \quad (4)$$

Since the determination of the magnetic-field vector components was performed at 24 points on the working orbit, we have from Eqs. (3) and (4) and the trapezium formula

$$\begin{aligned} \frac{\Delta(\mu_p/\mu_n)}{\mu_p/\mu_n} = & \left[ \frac{2\pi}{576H_0^2} \sum_{i=1}^{i=24} \Delta H_\phi(\varphi_i) (1 - \cos \varphi_i) \sum_{k=1}^{k=i} \Delta H_\rho(\varphi_k) \right] \\ & - \left[ \frac{1}{24H_0} \sum_{i=1}^{i=24} \Delta H_z(\varphi_i) (1 - \cos \varphi_i) \right] - \\ & - \left[ \frac{2\pi}{576H_0^2} \sum_{i=1}^{i=24} \Delta H_\rho(\varphi_i) \sin \varphi_i \sum_{k=1}^{k=i} \Delta H_\rho(\varphi_k) \right]. \end{aligned} \quad (5)$$

The magnetic-field components were determined by the compensation method discussed in detail in<sup>[13]</sup>. We used this method to determine  $\Delta H_z$  with an error which we could take into account by introducing the correction  $\Delta(\mu_p/\mu_n)_k/(\mu_p/\mu_n)$ , which we have called the compensation correction.<sup>[13]</sup> Therefore, the overall correction  $\Delta_1$  due to the magnetic field inhomogeneities can be written in the form

$$\Delta_1 = \frac{\Delta(\mu_p/\mu_n)}{\mu_p/\mu_n} + \frac{\Delta(\mu_p/\mu_n)_k}{\mu_p/\mu_n}. \quad (6)$$

Our measurements were performed at different magnet temperatures (between 19 and 25°C). The value of  $\Delta_1$  was different for different measurement runs because an increase in the magnet temperature resulted in a reduction in the field on the working orbit relative to the field at the center of the gap. This correction varied between  $-4.5 \times 10^{-4}$  and  $+6.3 \times 10^{-4}\%$ . The temperature correction was introduced into  $\Delta_1$  for each measurement run. The overall error associated with  $\Delta_1$  in the final measurement result was estimated at  $\pm 0.2 \times 10^{-4}\%$ .

## 2. Modulation Correction

Since the increase in the ion velocity in the modulator is not strictly a sinusoidal function, and the ions are accelerated over a small part of the path inside the modulator, the ion resonance frequency  $\omega_{\text{res}}$  was expressed in terms of the cyclotron frequency  $\omega_c$  by the following formula

$$\omega_{\text{res}} = \omega_c(n + p). \quad (7)$$

In this expression  $n = 196$  is the number of the harmonic of the cyclotron frequency on which the measurements are performed, and  $p$  is a small correction due to the above two factors.<sup>[3]</sup>

To determine  $p$  we obtained the exact equations of motion for an ion in the instrument, and the determination of  $p$  was reduced to the solution of a set of six transcendental equations. It was found<sup>[16]</sup> that for the parameters which we used in this work  $p = -0.0026766$ .

The final value of the modulation correction is  $\Delta_3 = p/196$  and amounts to  $-13.66 \times 10^{-4}\%$  of the final value  $\mu_p/\mu_n$ . Theoretical analysis showed that, for our precision of determining the modulator parameters, the error in the modulation correction was less than  $5 \times 10^{-6}\%$  of  $\mu_p/\mu_n$ .<sup>[16]</sup>

## 3. Relativistic Correction

For the ion velocities which we have employed, the relativistic change in the ion mass with velocity begins to be significant. The ion mass is given by

$$M = M_0/\sqrt{1 - (v/c)^2} \approx M_0(1 + 1/2v^2/c^2), \quad (8)$$

where  $M_0$  is the ion rest mass,  $v$  is the ion velocity, and  $c$  is the velocity of light. The relativistic change in the

mass will therefore produce a shift of the proton magnetic moment, expressed in nuclear magnetons, as follows:

$$(\mu_p/\mu_n)_{iM} = (\mu_p/\mu_n)_{iM} (1 - 1/2v_i^2/c^2), \quad (9)$$

where  $(\mu_p/\mu_n)_{iM}^*$  is the measured quantity and  $(\mu_p/\mu_n)_{iM_0}^*$  is the true value of the proton magnetic moment expressed in nuclear magnetons for the given type of ion  $i$ , corrected for the relativistic change in mass. The ion velocity on the working orbit is given by

$$v_i = rq_iH / M_i, \quad (10)$$

where  $r$  is the radius of the orbit,  $q_i$  and  $M_i$  are the charge and mass of the ion,  $H$  is the magnetic field, and  $c$  is the velocity of light. From this formula we have  $v_{\text{He}_4^+} \approx 3.26 \times 10^7$  cm/sec,  $v_{\text{Ne}_{20}^{++}} \approx 1.3 \times 10^7$  cm/sec,  $v_{\text{Ne}_{20}^+} \approx 0.652 \times 10^7$  cm/sec, and  $v_{\text{Ar}_{40}^+} \approx 0.326 \times 10^7$  cm/sec. Therefore, the relativistic change in mass shifts the  $(\mu_p/\mu_n)_{\text{He}_4^+}^*$  point by  $+0.6 \times 10^{-4}\%$ , whereas the  $(\mu_p/\mu_n)_{\text{Ne}_{20}^{++}}^*$  point is shifted by  $+0.096 \times 10^{-4}\%$ . The extrapolated value of  $(\mu_p/\mu_n)^*$  obtained from these two points, i.e., the value found for the pair  $\text{He}_4^+ - \text{He}_{20}^{++}$ , is shifted by  $\Delta_2 = -0.96 \times 10^{-4}\%$  from  $(\mu_p/\mu_n)^*$ , for the pair  $\text{He}_4^+ - \text{Ne}_{20}^{++}$  the shift is  $\Delta_2 = -0.75 \times 10^{-4}\%$ , and for  $\text{He}_4^+ - \text{Ar}_{40}^+$  it is found to be  $\Delta_2 = -0.67 \times 10^{-4}\%$  of  $(\mu_p/\mu_n)^*$ . The error in the correction for the relativistic change in mass combined with the error in the tabulated atomic masses was estimated as  $\pm 10^{-5}\%$  of  $\mu_p/\mu_n$ .

## 4. Correction for the Magnetic Properties of the Mass Spectrometer Chamber

Despite the fact that the RMMS chamber was produced from nonmagnetic brass and all the analyzer components were carefully checked for magnetic properties before insertion into the chamber, the introduction of the chamber into the magnet gap led to a certain distortion of the magnetic field at the ion orbit. This was probably connected with the fact that the permeability of the chamber material was not exactly equal to unity, and also to a substantial degree with the attraction to the magnet of some ferromagnetic components in the pumping system. The correction for the magnetic properties of the chamber was taken as the difference between the corrections for the magnetic field inhomogeneity with and without the chamber in the gap. The magnetic field distribution in the magnet gap with the chamber present was recorded with two NMR detectors, and the corrections for the magnetic properties of the lower part of the chamber and for its lid were determined separately. The correction for the chamber was  $+1.97 \pm 0.16 \times 10^{-4}\%$ , whereas the correction for the lid was  $+0.88 \pm 0.08 \times 10^{-4}\%$ . The total correction for the chamber with lid in position was  $\Delta_4 = +2.85 \pm 0.18 \times 10^{-4}\%$ .

Figure 7 shows all the extrapolation lines, and Table I summarizes the results of all the 11 measurement runs. The second column of the table shows the two types of ion which were simultaneously generated by the two-section ion source and whose cyclotron frequencies were measured in the given experiment. The third col-

FIG. 7. Extrapolation lines for all the measurement runs.

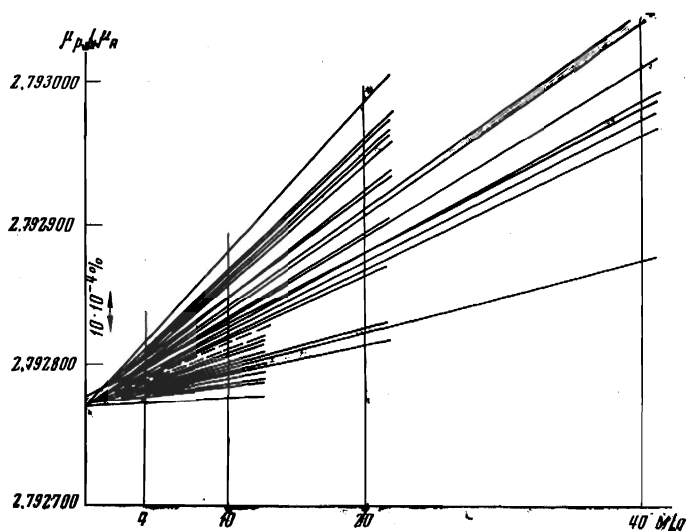


Table I. Results of measurements of  $\mu_p/\mu_n$

Run number	Ion pair	$(\mu_p/\mu_n)^*$	$\Delta_1 \times 10^4 \%$	$\Delta_2 \times 10^4 \%$	$\Delta_3 + \Delta_4 \times 10^4 \%$	$\sum_{i=1}^4 \Delta_i \times 10^4 \%$	$(\mu_p/\mu_n)^* + \sum_{i=1}^4 \Delta_i$	Mean $\mu_p/\mu_n$ for the run	Deviation from the mean $a_i \times 10^4$	Date of measurement
1	2	3	4	5	6	7	8	9	10	11
1	He <sub>4</sub> <sup>+</sup> — Ne <sub>20</sub> <sup>+</sup>	2.7928113	-0.30	-0.75	-10.81	-11.86	2.7927782	2.79277793	+3.53	25.2.71
	He <sub>4</sub> <sup>+</sup> — Ne <sub>20</sub> <sup>++</sup>	2.7928100		-0.96		-12.07	2.7927763			
	He <sub>4</sub> <sup>+</sup> — Ar <sub>10</sub> <sup>+</sup>	2.7928122		-0.67		-11.78	2.7927793			
2	He <sub>4</sub> <sup>+</sup> — Ne <sub>20</sub> <sup>+</sup>	2.7928045	+0.36	-0.75	-10.81	-11.20	2.7927732	2.79277343	-0.97	9.3.71
	He <sub>4</sub> <sup>+</sup> — Ne <sub>20</sub> <sup>++</sup>	2.7928055		-0.96		-11.41	2.7927736			
	He <sub>4</sub> <sup>+</sup> — Ar <sub>10</sub> <sup>+</sup>	2.7928046		-0.67		-11.12	2.7927735			
3	He <sub>4</sub> <sup>+</sup> — Ar <sub>10</sub> <sup>+</sup>	2.7928170	-4.44	-0.67	-10.81	-15.92	2.7927726	2.79277320	-1.20	11.3.71
	He <sub>4</sub> <sup>+</sup> — Ne <sub>20</sub> <sup>+</sup>	2.7928160		-0.75		-16.01	2.7927713			
	He <sub>4</sub> <sup>+</sup> — Ne <sub>20</sub> <sup>++</sup>	2.7928206		-0.96		-16.21	2.7927753			
4	He <sub>4</sub> <sup>+</sup> — Ar <sub>10</sub> <sup>+</sup>	2.7928180	-0.75	-0.67	-10.81	-15.92	2.7927736	2.79277540	+1.00	15.3.71
	He <sub>4</sub> <sup>+</sup> — Ne <sub>20</sub> <sup>+</sup>	2.7928098		-0.75		-12.31	2.7927754			
	He <sub>4</sub> <sup>+</sup> — Ne <sub>20</sub> <sup>++</sup>	2.7928070		-0.75		-11.09	2.7927760			
5	He <sub>4</sub> <sup>+</sup> — Ne <sub>20</sub> <sup>++</sup>	2.7928080	+0.47	-0.96	-10.81	-11.30	2.7927765	2.79277657	+2.27	5.5.71
	He <sub>4</sub> <sup>+</sup> — Ar <sub>10</sub> <sup>+</sup>	2.7928076		-0.67		-11.01	2.7927769			
	He <sub>4</sub> <sup>+</sup> — Ne <sub>20</sub> <sup>+</sup>	2.7928079		-0.75		-11.09	2.7927769			
6	He <sub>4</sub> <sup>+</sup> — Ne <sub>20</sub> <sup>+</sup>	2.7928025	+1.02	-0.75	-10.81	-10.54	2.7927731	2.79277275	-1.65	11.5.71
	He <sub>4</sub> <sup>+</sup> — Ne <sub>20</sub> <sup>++</sup>	2.7928020		-0.96		-10.57	2.7927724			
	He <sub>4</sub> <sup>+</sup> — Ar <sub>10</sub> <sup>+</sup>	2.7928032		-0.75		-10.70	2.7927733			
7	He <sub>4</sub> <sup>+</sup> — Ne <sub>20</sub> <sup>++</sup>	2.7928035	+0.86	-0.96	-10.81	-10.91	2.7927730	2.79277326	-1.14	13.5.71
	He <sub>4</sub> <sup>+</sup> — Ar <sub>10</sub> <sup>+</sup>	2.7928031		-0.67		-10.62	2.7927735			
	He <sub>4</sub> <sup>+</sup> — Ne <sub>20</sub> <sup>+</sup>	2.7928129		-2.88		-0.96	-10.81			
8	He <sub>4</sub> <sup>+</sup> — Ne <sub>20</sub> <sup>++</sup>	2.7928129	-4.21	-0.96	-10.81	-15.98	2.7927746	2.79277460	+0.20	24.5.71
	He <sub>4</sub> <sup>+</sup> — Ne <sub>20</sub> <sup>+</sup>	2.7927893		-0.75		-5.22	2.7927747			
	He <sub>4</sub> <sup>+</sup> — Ne <sub>20</sub> <sup>++</sup>	2.7927904		-0.96		-5.43	2.7927752			
10	He <sub>4</sub> <sup>+</sup> — Ar <sub>10</sub> <sup>+</sup>	2.7927893	+6.34	-0.67	-10.81	-5.14	2.7927749	2.79277498	+0.58	13.7.71
	He <sub>4</sub> <sup>+</sup> — Ne <sub>20</sub> <sup>+</sup>	2.7927897		-0.75		-5.22	2.7927751			
	He <sub>4</sub> <sup>+</sup> — Ne <sub>20</sub> <sup>++</sup>	2.7927909		-0.75		-5.70	2.7927750			
11	He <sub>4</sub> <sup>+</sup> — Ne <sub>20</sub> <sup>++</sup>	2.7927888	+5.86	-0.96	-10.81	-5.91	2.7927723	2.79277390	-0.50	14.7.71
	He <sub>4</sub> <sup>+</sup> — Ar <sub>10</sub> <sup>+</sup>	2.7927906		-0.67		-5.62	2.7927749			
	He <sub>4</sub> <sup>+</sup> — Ne <sub>20</sub> <sup>+</sup>	2.7927893		-0.75		-5.70	2.7927734			

Mean value  $\mu_p/\mu_n = 2.7927744$

umn gives the extrapolated value of  $(\mu_p/\mu_n)^*$  for the given pair of ions. The values given in this column correspond to a mean of 6–8 measurements. The root mean square deviation of the individual measurements from the mean  $(\mu_p/\mu_n)^*$  is less than  $0.2 \times 10^{-4}\%$  for all ion pairs in all runs. The fourth column of the table gives the overall correction  $\Delta_1$  for the magnetic-field inhomogeneity on the working orbit, taking into account all three components of the magnetic-field vector and the compensation correction. The fifth column gives the correction  $\Delta_2$  for the relativistic change in mass for the particular ion pair. Column six gives the uncertainty representing the modulation correction together with the correction for the magnetic properties of the chamber.

Column seven gives the sum of all the corrections which must be added to the extrapolated value of  $(\mu_p/\mu_n)^*$  in order to obtain the true value of  $\mu_p/\mu_n$  which, in turn, is given in column eight. Column nine gives the mean value of  $\mu_p/\mu_n$  for the run. Column ten gives the value of  $a_i$ , which is the deviation of the mean  $\mu_p/\mu_n$  for a given run from the overall mean obtained for all the eleven runs.

The mean value was found to be  $\mu_p/\mu_n = 2.7927744$ .

The root mean square deviation for a given run is

$$\sigma_{\text{rand}} = \sqrt{\sum a_i^2 / (N - 1)} = \pm 0.00000177 (\pm 0.64 \cdot 10^{-4}\%).$$

Analysis of the sources of random errors leads to a total root mean square error equal to the root mean

Table II. Possible systematic errors in the measured

Source of error	Root mean square error (in ten-thousandths %)
Asymmetry of the cyclotron peak (1% of width)	0.20
Error in the correction for the magnetic field susceptibility:	0.20
Error in the correction for magnetic field in-bility:	
RMMS chamber	0.16
chamber lid	0.08
Error in the correction for the relativistic change in the ion mass, including uncertainty in the atomic masses	0.10
Error due to the magnetic effect of the cathode current	0.10
Overall error $\sigma_c = \sqrt{\sum_{s=1}^5 \sigma_s^2}$	$\sim 0.37$

square deviation of the results obtained in the individual runs from the overall mean. The random error in the arithmetic mean of N runs is

$$\sigma_{\bar{\mu}} = \frac{\sigma_{\text{rand}}}{\sqrt{N}} \approx 0.20 \cdot 10^{-4} \%$$

Table II shows the possible systematic errors common to all the runs. Since they are mutually independent, we can apply to them the rule for the combination of variances and, therefore, the overall error can be found from

$$\sigma_c = \sqrt{\sum \sigma_s^2},$$

where  $\sigma_s$  represents the individual systematic errors. It amounts to  $\sim 0.37 \times 10^{-4} \%$ . The resultant root mean square error due to random and possible systematic errors is given by

$$\sigma_n = \sqrt{\sigma_r^2 + \sigma_c^2}$$

and amounts to  $\sim 0.43 \times 10^{-4} \%$ .

Therefore, the final result, given without correction for the diamagnetic screening of the proton in the water molecule, is

$$\mu_p / \mu_n = 2.7927744 \pm 0.0000012 (\pm 0.43 \cdot 10^{-4} \%).$$

## V. CONTROL EXPERIMENTS

A number of control measurements were performed to verify the validity of the above results.

1. By varying the partial pressures of the gas components, it was shown that the final result was independent of changes in the polarization potentials produced by ions in the drift space between the modulator and the drift slit.

2. By varying the amplitude of the modulating voltage it was shown that a change in the modulation conditions within a range clearly exceeding possible errors in establishing the calculated parameters has no effect on the final result to within our experimental error. This also follows from a theoretical calculation of the modulation corrections.<sup>[16]</sup>

3. A check was made on the effect of the state of the surface of the chamber on the final result. Most of these measurements were performed with the inner surface of the chamber covered with aquadag. Two runs (runs 8 and 9 in Table I, dashed lines in Fig. 7) were performed with all the screens having clean copper surfaces. The

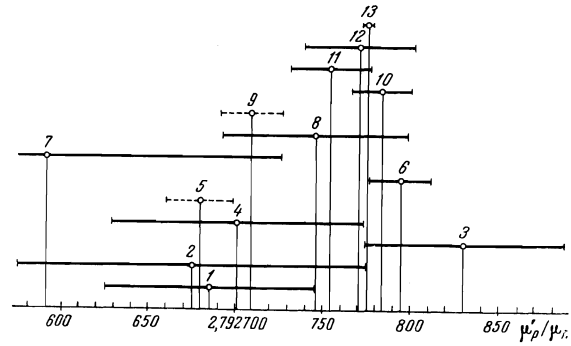


FIG. 8. Summary of all the results of various measurements of  $\mu_p/\mu_n$ : 1—[12], 2—[18,19], 3—[5], 4—[20], 5—[2], 6—[3], 7—[21], 8—[22], 9—[1], 10—[8], 11—[6], 12—[7], 13—present work.

results of these two runs were in complete agreement with other measurements.

4. It was verified that the final results of the measurements were independent of the magnetic field sweep amplitude.

5. It was verified that the leakage of electric fields from the ion source had no effect.

6. It was verified that eddy currents which appeared when the chamber was introduced into the magnet gap had no effect on the magnetic-field profile.

7. Since the corrections for the magnetic susceptibility of the lid and chamber of the RMMS were determined separately, there was no need to check for the influence of the shunting effect of the thick ring-shaped wall of the chamber on the distribution of the magnetic field on the ion orbit. Measurements showed that the total correction for the magnetic susceptibility of the RMMS lid and chamber taken separately agreed with the correction for the magnetic susceptibility of the assembled chamber to within  $10^{-5} \%$ .

8. It was verified that any possible shift in the position of the chamber in the magnet gap had no effect on the final result of the measurements.

9. It was verified that possible stray magnetic fields in the room in which the measuring installation was located had no effect on the final measurement results.

10. By comparing the NMR frequency for a pure water specimen with the NMR frequency for a water specimen containing 0.3 g/liter of the paramagnetic salt  $\text{CuCl}_2$ , it was verified that this salt had no effect on the NMR frequency.

The above control experiments and our analysis of random errors lead us to believe that our measurements are free from the effect of any appreciable sources of systematic errors and that the true error is close to that indicated in our final result.

## VI. CONCLUSIONS

Figure 8 shows all the measurements of  $\mu_p/\mu_n$  available at present. The error bars represent the root mean square error as reported by the various workers. The broken lines represent values of  $\mu_p/\mu_n$  obtained as a result of the 1963–64<sup>[2]</sup> and 1969<sup>[1]</sup> reconciliation of the fundamental constants.

The value of  $\mu_p/\mu_n$  obtained in the present work agrees to within experimental error with the results of

Gubler et al.,<sup>[7]</sup> Petley and Morris,<sup>[6]</sup> Fystrom,<sup>[8]</sup> and Mamyryn and Frantsuzov.<sup>[3]</sup>

It may therefore be concluded that the so-called "high values" of  $\mu_p/\mu_n$  are experimentally better founded than the "low values", contrary to the conclusion reached by Taylor et al.<sup>[1]</sup>

Our result differs from the value of  $\mu_p/\mu_n$  obtained as a result of the 1969 reconciliation of constants<sup>[1]</sup> by  $23 \times 10^{-4}\%$ . The ratio  $\mu_p/\mu_n$  is closely connected with the Faraday constant  $F$ , the Avogadro number  $N$ , the proton charge-to-mass ratio  $e/m_p$ , and the proton gyromagnetic ratio  $\gamma_p$ :

$$\mu_p/\mu_n = \gamma_p M_p / F = c \gamma_p m_p / e, \quad F = Ne/c.$$

Hence it is clear that the acceptance of a value for  $\mu_p/\mu_n$  close to that reported in our previous paper<sup>[17]</sup> will have a considerable effect on the entire system of fundamental constants.<sup>1)</sup>

We are currently planning a number of further series of measurements in order to improve further the accuracy of our measurements of the proton magnetic moment in nuclear magnetons. One of the principal problems will be to investigate the possible effect of the correlation between the slopes of the extrapolation lines and the values of  $(\mu_p/\mu_n)^*$  determined from these lines. It is also necessary to elucidate the possible small non-linearity of the extrapolation lines. However, the expected effect can modify the mean value  $\mu_p/\mu_n$  only by an amount substantially smaller than the uncertainty which we have indicated above.

<sup>1)</sup>The final result reported in [17] is slightly different from that reported here because we have since improved the modulation correction (see [16]).

<sup>1</sup>V. N. Taylor, W. H. Parker, and D. N. Langenberg, *Rev. Mod. Phys.* **41**, 375 (1969).

<sup>2</sup>E. R. Cohen and J. W. M. Du Mond, *Rev. Mod. Phys.* **37**, 537 (1965).

<sup>3</sup>B. A. Mamyryn and A. A. Frantsuzov, *Zh. Eksp. Teor. Fiz.* **48**, 416 (1965) [*Sov. Phys.-JETP* **21**, 274 (1965)].

<sup>4</sup>D. N. Craig, J. I. Hoffman, C. A. Law, and W. J. Hamer, *J. Res. NBS* **64A**, 381 (1960).

<sup>5</sup>H. S. Boyne and P. A. Franken, *Phys. Rev.* **123**, 242 (1961).

<sup>6</sup>B. W. Petley and K. Morris, *Proc. Intern. Conf. on Precision Measurement and Fundamental Constants*, NBS, Gaithersburg, Maryland, USA, August, 1970, p. 173.

<sup>7</sup>H. Gubler, W. Reichart, M. Roush, H. Staub, and F. Zamboni, *Proc. Intern. Conf. on Precision Measurements and Fundamental Constants*, NBS, Gaithersburg, Maryland, USA, August, 1970, p. 177.

<sup>8</sup>D. O. Fystrom, *Phys. Rev. Lett.* **25**, 1469 (1970).

<sup>9</sup>A. Loesche, *Nuclear Induction* (Russ. Transl.), IIL, 1963.

<sup>10</sup>B. A. Mamyryn and A. A. Frantsuzov, *Prib. Tekh. Eksp.*, No. 3, 114 (1962).

<sup>11</sup>B. A. Mamyryn and A. A. Frantsuzov, *Dokl. Akad. Nauk SSSR* **159**, 777 (1964) [*Sov. Phys.-Dokl.* **9**, 1082 (1965)].

<sup>12</sup>H. Sommer, H. A. Thomas, and J. A. Hipple, *Phys. Rev.* **82**, 697 (1951).

<sup>13</sup>B. A. Mamyryn, N. N. Aruev, and S. A. Alekseenko, *Izmeritel'naya Tekhnika* **10** (1972).

<sup>14</sup>J. H. E. Mattauch, W. Thiele, and A. H. Wapstra, *Nucl. Phys.* **67**, 1 (1965).

<sup>15</sup>B. A. Mamyryn, *Doctoral Dissertation*, FTI, Leningrad, 1966.

<sup>16</sup>S. A. Alekseenko, N. N. Aruev, B. A. Mamyryn, A. A. Frantsuzov, and M. P. Proskura, *Izmeritel'naya Tekhnika* **9** (1972).

<sup>17</sup>B. A. Mamyryn, N. N. Aruev, and S. A. Alekseenko, Paper read to the Fourth International Conference on Atomic Masses and Fundamental Constants, Teddington, Middlesex, England, September, 1971.

<sup>18</sup>F. Bloch and C. D. Jeffries, *Phys. Rev.* **80**, 305 (1950).

<sup>19</sup>K. R. Trigger, *Bull. Amer. Phys. Soc.* **2**, 220 (1956).

<sup>20</sup>J. H. Sanders and K. C. Turberfield, *Proc. Roy. Soc., London* **A272**, 79 (1963).

<sup>21</sup>J. B. Marion and H. Winkler, *Phys. Rev.* **156**, 1062 (1967).

<sup>22</sup>B. W. Petley and K. Morris, *Proc. Third Intern. Conf. on Atomic Masses*, University of Manitoba Press, Winnipeg, Canada, 1968, p. 461.

Translated by S. Chomet